6p

PHASE SEGREGATION DUE TO SIMULTANEOUS MIGRATION AND COALESCENCE

Robert H. Davis, Hua Wang, and Debra Hawker
Department of Chemical Engineering
University of Colorado
Boulder, Colorado 80309-0424

ABSTRACT

Ground-based modeling and experiments have been performed on the interaction and coalescence of drops leading to macroscopic phase separation. The focus has been on gravity-induced motion, with research also initiated on thermocapillary motion of drops. The drop size distribution initially shifts toward larger drops with time due to coalescence, and then back towards smaller drops due to the larger drops preferentially settling out. As a consequence, the phase separation rate initially increases with time and then decreases.

INTRODUCTION

Dispersions of drops of one fluid in a second, immiscible fluid are frequently encountered in industrial and natural processes such as extraction, rain-drop growth, food and beverage processing, and the formation of liquid-phase-miscibility-gap materials. In the absence of stirring or bulk motion, dispersed drops of different sizes may undergo relative motion under the action of gravity. The larger drops migrate more rapidly and catch up to the smaller drops in their path, leading to possible contact and coalescence. In a finite sample, drop migration and coalescence generally result in an inhomogeneous dispersion with phase separation. In extraction, this is the desired result; the two phases must separate subsequent to mixing for the partitioned component to be recovered. A counter-example is the processing of liquid-phase-miscibility-gap metals, for which the desired product is a composite material with fine particles of one metal uniformly dispersed in a matrix of the other. Low-gravity environments suppress buoyancy-driven droplet motion, but coalescence and phase separation may still occur due to thermocapillary effects [1].

Gravity sedimentation of particles in the absence of coalescence or aggregation has been studied extensively [2]. Similarly, coalescence of drops in spatially uniform dispersions in the absence of phase separation has been modeled extensively [3-6]. A notable example of simultaneous sedimentation and coalescence is the study of Reddy, Melik & Fogler [7]. They noted that the probability size distribution shifts toward larger drops when coalescence dominates, toward smaller particles when sedimentation dominates, and initially toward larger drops and subsequently toward small drops when both mechanisms are important.

In the current work, we predict the macroscopic phase separation and drop-size distributions for buoyancy-driven sedimentation and coalescence of immiscible dispersions of drops by solving the general population dynamics equations with both time-dependence and spatial-dependence retained, and incorporating a mass balance on the drops arriving at the moving interface. Preliminary experiments on two-phase systems are also presented. Comparison work has been performed on drop coalescence due to Brownian diffusion and thermocapillary effects, with the focus to-date on spatially uniform dispersions [5,6,8].

THEORY

We consider a dilute dispersion of spherical drops of viscosity μ' and density ρ' dispersed in an immiscible fluid of viscosity μ and density ρ. The drops are considered to be nonBrownian, but not so large that inertial effects or deformation are important. For common liquids, these conditions are met for drops with diameters of 2-100 μm [9].

The typical problem of interest is illustrated in Fig. 1. The initial condition (Fig. 1a) is a uniform suspension of droplets of one fluid dispersed in a second, immiscible liquid. After mixing is stopped, the drops begin to rise due to buoyancy (assuming, for illustrative purposes, that $\rho' < \rho$). As the drops reach the top of the container, they coalesce into an overlying, segregated layer of the dispersed-phase fluid (Fig. 1b). This layer grows with time (Fig. 1c) until all of the dispersed drops have coalesced into it (Fig. 1d). The problem is complicated by the possibility that the drops also collide and coalesce with each other as they rise, and, because the larger drops move faster and leave the smaller ones behind, the drop size distribution varies with both time and position.

The temporal and spatial evolutions of the drop size distribution are studied by using population dynamics equations:

$$\frac{\partial n_i}{\partial t} + \frac{\partial (u_i n_i)}{\partial z} = \frac{1}{2} \sum_{j=1}^{i-1} J_{j(i-j)} - \sum_{j=1}^{N} J_{ij} \quad , \qquad i = 1, 2, \ldots N \quad , \tag{1}$$

where n_i is the number of drops per unit volume in the discrete size category i, u_i is the Stokes' settling velocity of drops of size i, t is time, z is the direction of drop migration (vertical, as defined in Fig. 1), J_{ij} is the rate of collisions per unit volume of size i drops with size j drops, and N is the total number of size categories. The first term on the right-hand-side of Eq. (1) is the rate of formation of size i drops by collision of two smaller drops, and the second term is the rate of loss of size i drops due to their collisions to form larger drops. The collision rate between drops in size category i (larger drops) and the size category j (smaller drops) may be expressed as [9]:

$$J_{ij} = n_i n_j \pi (a_i + a_j)^2 \mid u_i - u_j \mid E_{ij} \quad , \tag{2}$$

where a_i and a_j are the large and small drop radii, respectively, and E_{ij} is the collision efficiency. The collision efficiency equals unity when the drops move independently until colliding; values of E_{ij} differing from unity are given previously [9] and account for hydrodynamic forces which cause the drops to move around one another and the attractive forces which pull them together.

The rate at which the lighter phase grows at the top of the vessel due to droplets reaching this phase is determined by a mass balance:

$$-A \frac{dh_u}{dt} = \sum_{i=1}^{N} A \left(u_i - \frac{dh_u}{dt} \right) n_i V_i \quad , \tag{3}$$

where the left-hand-side is the rate of accumulation of the upper phase and the right-hand-side is the flux of drops into the upper phase, A is the cross-sectional area of the container, $V_i = \frac{4}{3}\pi a_i^3$ is the volume of a drop of size i, and $\phi = \sum_{i=1}^{N} V_i n_i$ is the total volume fraction of droplets in the suspension just below the upper interface at $z = h_u(t)$. The initial condition is $h_u = H$ at $t = 0$.

The population dynamics equations were nondimensionalized and then solved using the Lax-Wendroff finite-difference method [10]. The numerical methods used in the modeling involve logarithmic discretization of drop spectra into N categories which have equal spacing in the logarithm of droplet mass or volume, and the mass or volume of a droplet within each discrete category doubles every fourth category [3]. The initial size distributions, assumed uniform for $0 \leq z \leq H$, were chosen to be normal distributions on a number basis, as specified by the number-averaged drop radius, a_o, and the standard deviation, σ, of drop radii. In dimensionless form, normal distributions are characterized by a single dimensionless parameter, $\hat{\sigma} = \sigma / a_o$. The dimensionless parameters which affect the macroscopic behavior of a dispersion include the viscosity ratio, $\hat{\mu} = \mu'/\mu$, the dimensionless standard deviation of radii in the initial distribution, $\hat{\sigma} = \sigma/a_o$, the initial volume fraction, ϕ_o, and the time scale ratio, $N_\tau \equiv \tau_s/\tau_c = 3\phi_o H/4a_o$, where $\tau_s = H/u_o$ is the characteristic settling time for drop with velocity u_o and radius a_o to travel the length of the container, and $\tau_c = 4a_o/(3\phi_o u_o)$ is the characteristic coalescence time.

Figure 2 shows the evolution of the average radius (defined in [5] as the radius of a drop having the mass-averaged volume) versus time at the container midpoint for a dispersion having $\hat{\sigma} = 0.2$, $\hat{\mu} = 0.1$, and different values of N_τ. It is seen that the average droplet radius initially increases with time due to coalescence; after the larger drops sediment out of the dispersion, the average radius began to decrease.

The variation of the droplet volume fraction with dimensionless position at different times is shown in Fig. 3 for a dispersion with $\hat{\mu} = 0.1$, $\hat{\sigma} = 0.2$, and N_τ=20. The volume fraction in the lower regions of the container decreases rapidly with time as the drops rise. For short times, the volume fraction in the upper regions of the dispersion is the same as the initial volume fraction. This is because droplets which rise out of a control volume at the top of dispersion are replaced at an equal rate by droplets moving into the control volume. With time increasing, however, larger drops rise out of the dispersion, and the volume fraction at any height in the dispersion system is significantly less than the initial volume fraction.

Typical results for the gravitational phase separation rate are shown in Fig. 4 for a dispersion having $\hat{\mu} = 0.1$, $\hat{\sigma} = 0.1$ (dashed lines), $\hat{\sigma} = 0.2$ (solid lines), ϕ_o=0.05, and different N_τ. When N_τ=0, no coalescence occurs. Phase separation then takes place at a constant rate until the largest drops rise out of the dispersion, after which the phase separation rate monotonically decreases due to fewer and smaller drops arriving at the phase interface. When $N_\tau > 0$, the phase separation rate initially increases, because coalescence leads to larger drops with faster rise rates. Once these drops rise out of suspension, however, the phase separation rate reaches a maximum and then decreases as only smaller drops remain. Note that relatively large values of $N_\tau \geq O(10)$ are necessary for coalescence to significantly affect the phase separation process. This is because typical collision efficiencies are $O(10^{-1})$ for dispersions with $\hat{\mu} = 0.1$ [9].

EXPERIMENTS

Experiments to observe and measure drop coalescence and phase segregation due to gravity sedimentation have been initiated with two phase systems: 1,2-propanediol drops in dibutyl sebacate, and an aqueous biphase mixture containing 1% dextran (MW = 500) and 6.5% polyethylene glycol (PEG, MW = 8000) by weight. The experiments were carried out in an optical cuvette of 1 cm × 1 cm cross-section, with heights up to 20 cm. Before transferring the two phases to the cuvette, vortexing was performed twice for one minute each. This resulted in a range of drop diameters of approximately 5-30 μm. The height of the segregated minority phase was followed as a function of time using a videomicroscope connected to a video recorder and a personal computer containing Global Lab Image analysis software by Data Translation. For the aqueous biphase system, samples at various heights were taken using inserted syringes and analyzed for the volume fraction of the droplet phase.

The experimental results are in qualitative agreement with the theory; quantitative comparison has not yet been made. Figure 5 shows a plot of the height of the segregated droplet phase, normalized by the final height it achieves after complete separation, versus time for two values of the total height of the 1,2-propanediol/dibutyl sebacate dispersion: $H = 10$ cm and $H = 14.5$ cm. In both cases, a sigmoidal-shaped curve is observed, as expected. The initial phase separation rate is slow because of the small drop sizes and velocities; it then speeds up as coalescence occurs to yield larger drops, and then it decreases again as the large drops settle out of the dispersion. As predicted from Fig. 4, the phase separation is faster for the taller dispersion (N_τ greater) because there is more opportunity for coalescence. At a given position, the observed drop size increased initially due to coalescence and then decreases due to sedimentation of the larger drops, as predicted in Fig. 2, but quantitative analysis of the drop size distributions has not yet been performed.

Similar results have been obtained with the aqueous biphasic system. Figure 6 shows the volume percent of minority phase versus distance from the bottom of the cuvette for a total minority phase volume percent of 6.5% and total height of the dispersion of $H = 17$ cm. Note that the minority, dextran-rich phase is more dense than the continuous, PEG-rich phase, and so the droplets settle downward. Similar to the behavior predicted in Fig. 3, the droplet volume fraction is uniform and equal to its initial value for short times and

then decreases with time. The decrease occurs first in the upper portion of the container, due to droplets settling downward.

CONCLUSIONS

Quantitative predictions of the temporal and spatial evolutions of the drop size distributions and macroscopic phase separation rates in droplet dispersions due to buoyancy-driven motion are presented. Droplet coalescence significantly increases the phase separation rate initially, and then the phase separation rate decreases after the larger drops are removed from the dispersion. The predicted trends are verified by experiments.

ACKNOWLEDGMENTS

This work was supported by NASA grant NAG3-1389. The authors thank two undergraduate assistants, Tyler Kinkade and Nathan Reader, for assistance with the experiments.

REFERENCES

1. Bergman, A., Fredriksson, H., & Shahani, H., The effect of gravity and temperature gradients on precipitation in immiscible alloys. *J. Mat. Sci.* **23** (1988) 1573-1579.

2. Davis, R.H. & Acrivos, A. Sedimentation of noncolloidal particles at low Reynolds numbers. *Ann. Rev. Fluid Mech.* **17** (1985) 91-118.

3. Rogers, J.R. & Davis, R.H. Modeling of collision and coalescence of droplets in microgravity processing of Zn-Bi immiscible alloys. *Metallurgical Trans.* **21A** (1990) 59-98.

4. Satrape, J.V. Interactions and collisions of bubbles in thermocapillary motion. *Phys. Fluids A* **4** (1992) 1883-1900.

5. Wang, H. & Davis, R.H. Droplet growth due to Brownian, gravitational, or thermocapillary motion and coalescence in dilute dispersions *J. Colloid Interface. Sci.* **159** (1993) 108-118.

6. Zhang, X., Wang, H. & Davis, R.H. Collective effects of temperature and gravity on droplet coalescence *Physics of Fluids A* **5** (1993) 1602-1613.

7. Reddy, S.R., Melik, D.H. & Fogler, H.S. Emulsion stability-theoretical studies on simultaneous flocculation and creaming. *J. Colloid Interface Sci.* **82** (1981) 116-127.

8. Zhang, X. & Davis, R.H. The collision rate of small drops due to thermocapillary migration *J. Colloid Interface Sci.* **152** (1992) 548-561.

9. Zhang, X. & Davis, R.H. The collisions of small drops due to Brownian and gravitational motion *J. Fluid Mech.* **230** (1991) 479-504.

10. Lax, P.D. & Wendroff, B. 1960 Systems of conservation laws. *Comm. Pure Appl. Meth.* **13** (1960) 217-237.

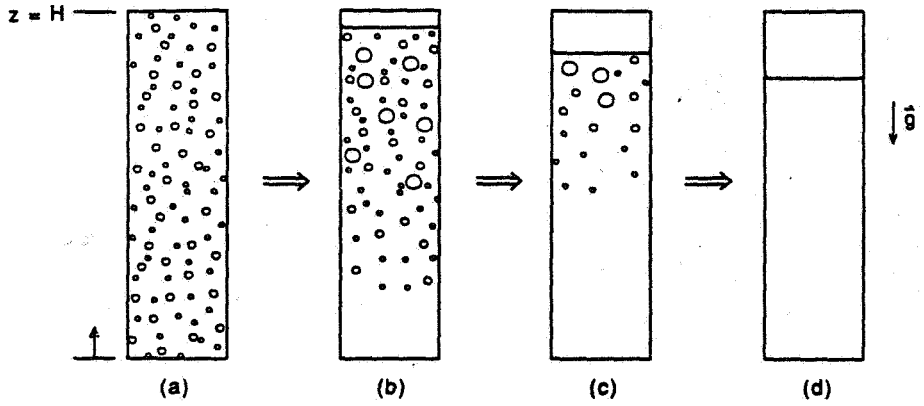

Fig. 1–Schematic of the time evolution of the phase separation process due to the simultaneous migration and coalescence of rising drops or bubbles.

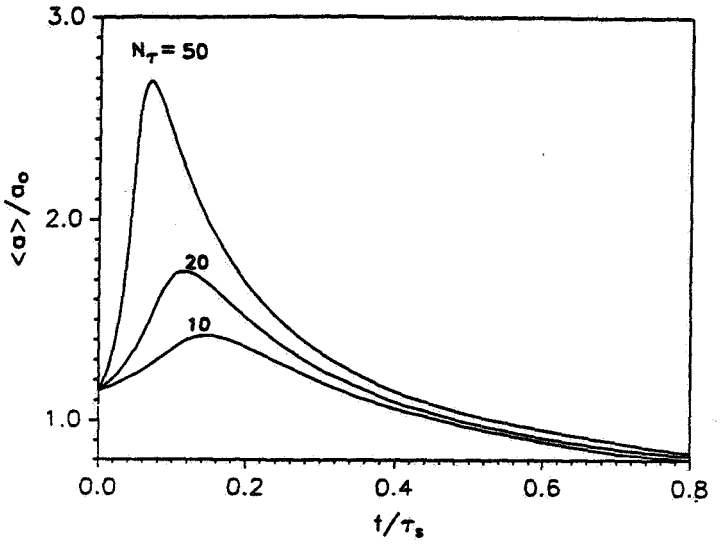

Fig. 2–Predicted time evolution of the average drop radius at $z/H = 0.5$ for a dispersion having $\hat{\mu}$=0.1 and $\hat{\sigma}$=0.2.

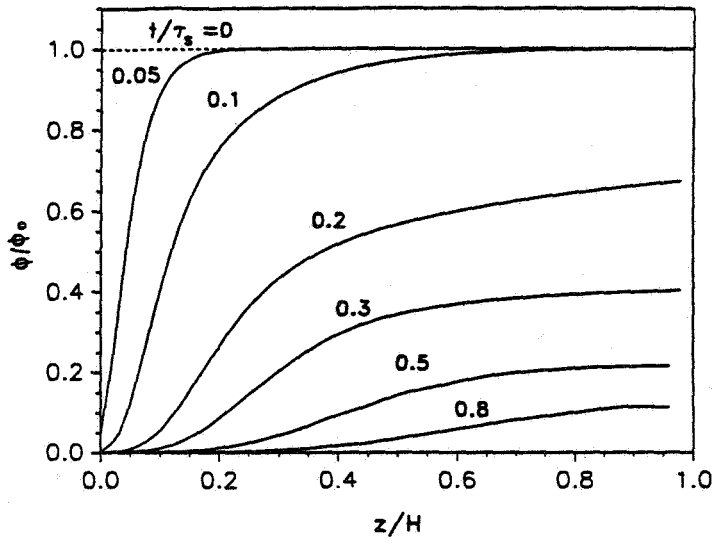

Fig. 3–Predicted variation of volume fraction with position at different times for a dispersion having $\hat{\mu} = 0.1$, $\hat{\sigma} = 0.2$, and $N_T = 20$.

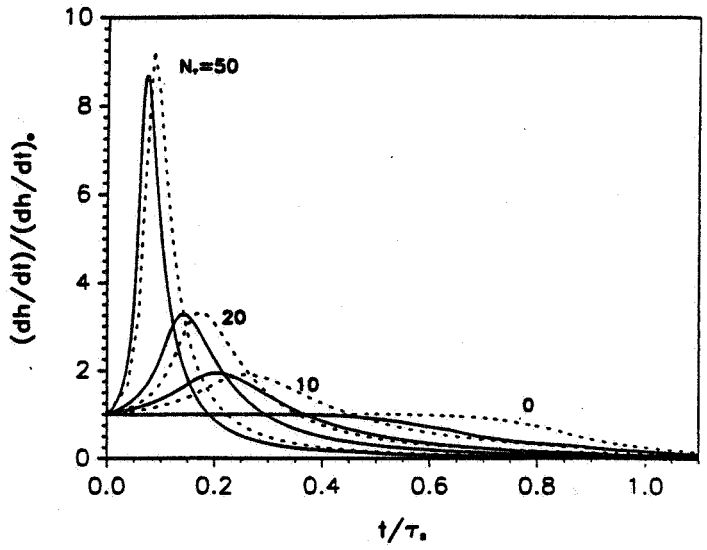

Fig. 4–Predicted rate of phase separation versus time for a dispersion having $\hat{\mu} = 0.1$, $\hat{\sigma} = 0.2$ (solid lines), $\hat{\sigma} = 0.1$ (dashed lines), $\phi_o = 0.05$ and different N_τ in a container of finite depth.

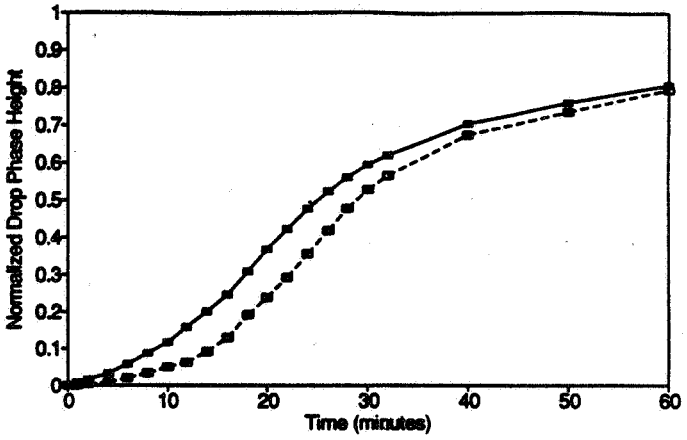

Fig. 5–Measured height of segregated minority phase (normalized by final height) versus time for 1,2-propanediol drops at $\phi_o = 0.034$ in dibutyl sebacate with H=10 cm (open squares) and H = 14.5 cm (closed squares).

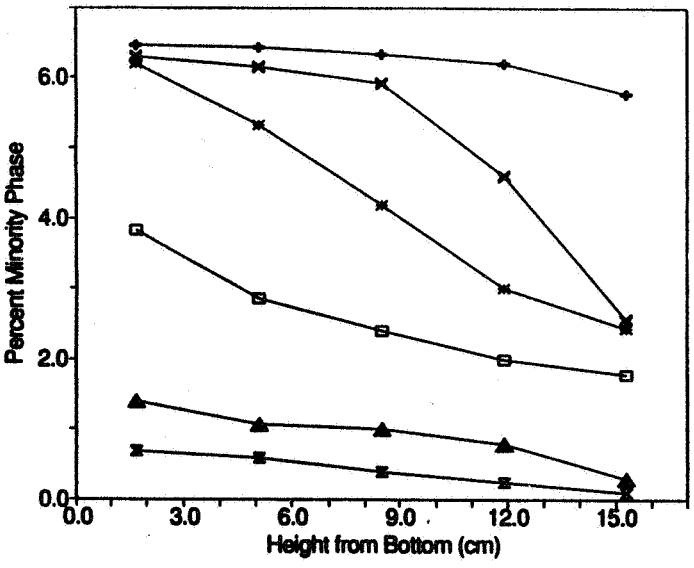

Fig. 6–Volume percentage of dispersed phase versus distance from the bottom of the curvette for dextran-rich drops at $\phi_o = 0.065$ in PEG-rich continuous phase with H = 17 cm at t = 15, 30, 45, 60, 120, and 240 min (top to bottom).